Gas Multiple Flow Mechanisms and Apparent Permeability evaluation in Shale Reservoirs

Xuelei Feng[1,2,3], Ruiqi Duan[1,2,3]

1. Institute of Geology and Geophysics, Chinese Academy of Sciences; 2. Institutions of Earth Science, Chinese Academy of Sciences; 3. University of Chinese Academy of Sciences.

The large-scale exploitation of shale gas benefited from successful implementation of hydraulic fracturing. Shale reservoir is referred to as the heterogeneous porous media with nano-matrix and multi-scale fractures. Considering the collision between gas molecules and the collisions between gas molecules and the surface of nanopore walls, gas flow in nanoscale confined space exhibits non–continuum effects. Thus, gas flow mechanisms and apparent permeability are important factors for predicating and valuating gas production in shale stimulated reservoirs.

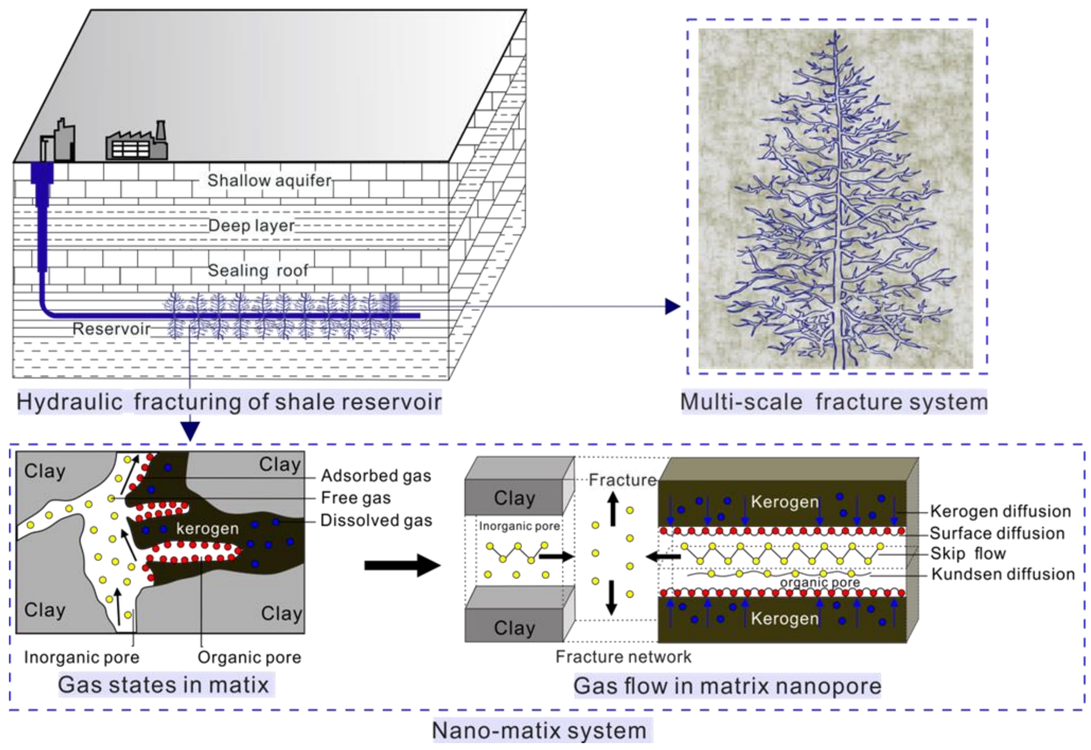

Figure 1. Gas multiple flow mechanisms in stimulated shale reservoir [1-3].

Multiple flow mechanisms in shale nanopores include kerogen diffusion, surface diffusion, Knudsen diffusion, transmit flow, and slip flow. The characterization of gas flow mechanisms frequently depend on the Knudsen number to evaluate whether Knudsen diffusion, slip flow, transitional flow, or continuous flow exists in nanopores of tight reservoirs. While, different flow mechanisms are characterized separately.

Surface diffusion:

$$J_s = -D_s \frac{\xi_{ms} c_s}{p} \nabla p$$

Knudsen diffusion:

$$J_S^{'} = -(1+\frac{b}{p}) \frac{r^2 \rho^2}{8\mu} \nabla p$$

Slip flow:

$$J_K = -\frac{M D_K}{10^3 RT} \nabla p$$

Transitional flow:

$$J_T = J_K + J_S^{'}$$

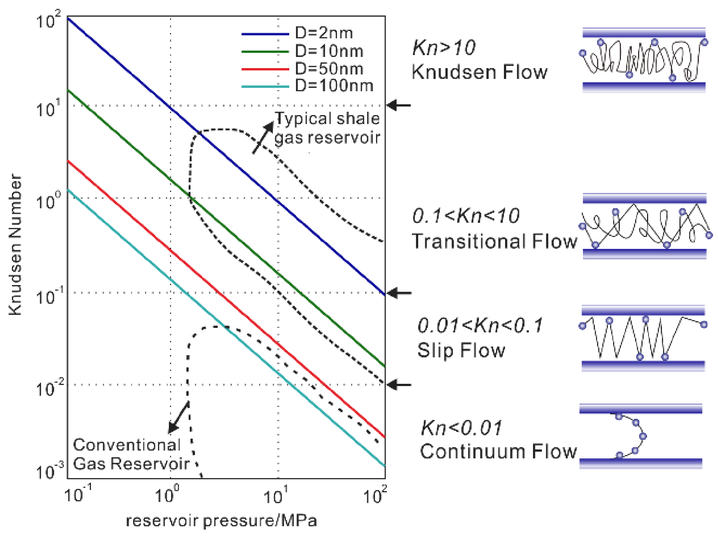

Figure 2. Gas flow regimes predominated by the Knudsen number [1].

The total flow mass through nanopore by the combination of dynamic flow regimes is:

$$J = -(D_s \frac{\xi_{ms} C_s}{p} + \frac{2rM}{3\times10^3 RT}\left(\frac{8RT}{\pi M}\right)^{0.5} + (1+\frac{b}{p})\frac{r^2\rho^2}{8\mu})\nabla p$$

Considering macroscopic scales of stimulated reservoir and fractures as the main seepage channels, the total volumetric based on Darcy equation is:

$$k_{app} = D_s \frac{\xi_{ms} C_s \mu}{p\rho^2} + \frac{2r\mu M}{3\times10^3 \rho^2 RT}\left(\frac{8RT}{\pi M}\right)^{0.5} + (1+\frac{b}{p})\frac{r^2}{8}$$

We divided dynamic permeability by Darcy permeability type:

$$\frac{k_{app}}{k_d} = D_s \frac{\xi_{ms} C_s \mu}{p\rho^2}\frac{8}{r^2} + \frac{2\mu M}{3\times10^3 \rho^2 RT}\left(\frac{8RT}{\pi M}\right)^{0.5}\frac{8}{r} + (1+\frac{b}{p})$$

The 2D time–dependent Rock Mechanic module and Subsurface Flow module in COMSOL are applied to simulate the gas flow process. A constant pressure was applied to the left and right boundaries of the model, which were considered the interface between the fracture and the matrix.

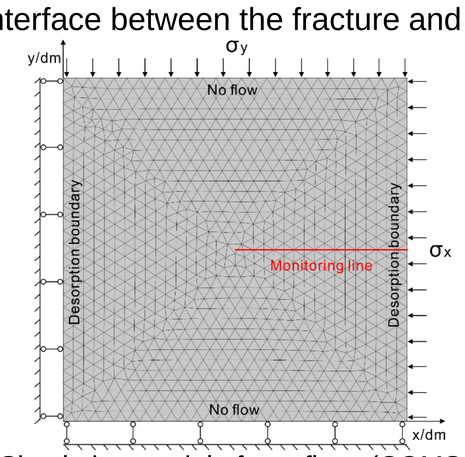

Simulation model of gas flow (COMSOL solver)

Parameters of simulation model

Parameter	Value
Young's modulus of shale, E (GPa)	30
Poisson's ratio of shale, ν	0.2
Density of shale, ρ_s (kg/m^3)	2700
Average pore diameter of matrix, $\bar{d}$ (nm)	10
Density of gas, ρ_g (kg/m^3)	0.717
Viscosity of gas, μ (Pa·s)	2×10^4
Molar mass of gas, M (kg/mol)	0.016
Gas molecular diameter, d_m (nm)	0.38
Reservoir initial pressure, P (MPa)	30
Overburden pressure, σ_y (MPa)	50
Confining pressure, σ_x (MPa)	53
Boundary pressure, P_0 (MPa)	10
Langmuir pressure constant, P_L (MPa)	4
Langmuir volume constant, V_L (m^3/kg)	3×10^{-3}
Initial porosity of matrix, ϕ_0	0.05
Initial permeability of matrix, k_0 (m^2)	1×10^{-18}
Standard molar volume, V_0 (L/mol)	22.4
Avogadro constant, N_A (mol^{-1})	6.02×10^{23}

The matrix block pressure distribution is shown with different pore sizes and production times. With gas production, the pressure of the matrix block near the outflow boundary slowly becomes equal to the fracture pressure. The pore size significantly affects the reservoir pressure distribution. An increased pore size of the shale promotes rapid penetration of gas under a drop in pressure. The shale block pressure rapidly decreases to the fracture pressure. This suggests that more intensive fractures should be developed to obtain more gas.

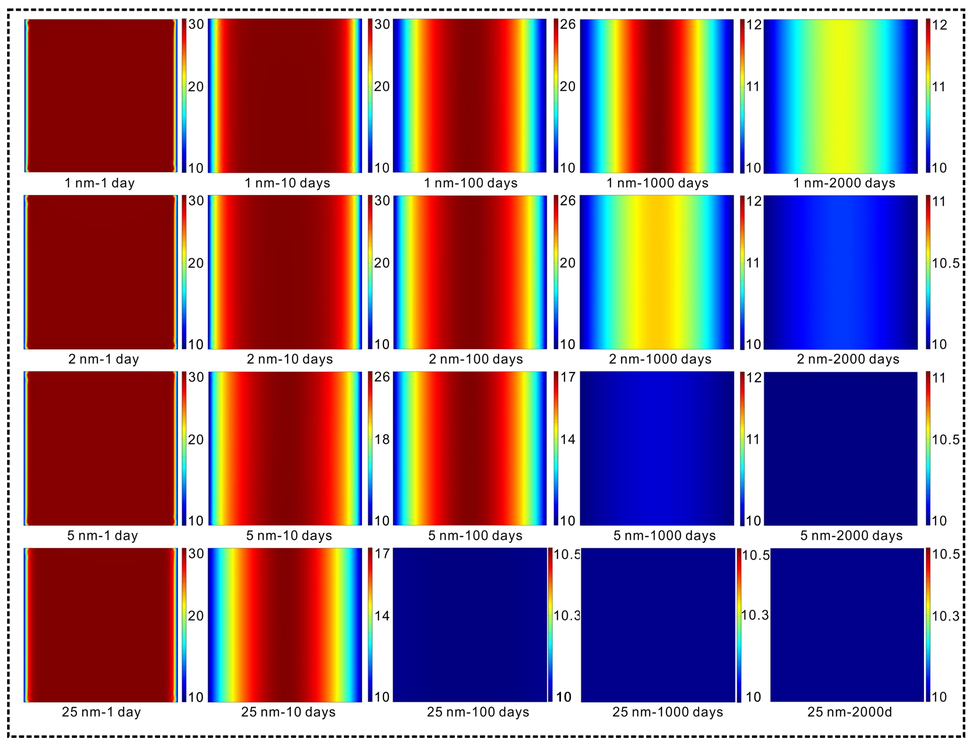

Figure 3. Shale block pressure distribution (MPa) at different pore radii (nm) and production times (days)

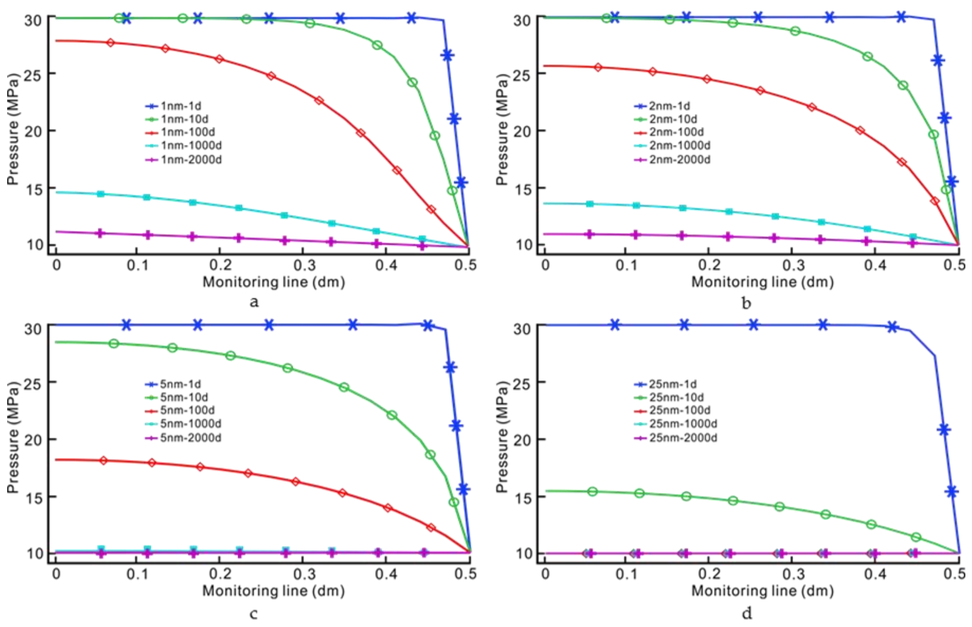

Figure 4. Pressure distribution on the monitoring line: (a) pore radius = 1 nm; (b) pore radius = 2 nm; (c) pore radius = 5 nm; (d) pore radius = 25 nm.

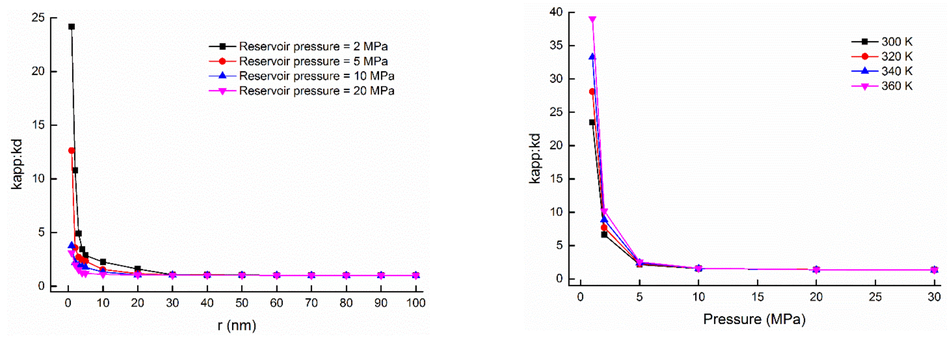

Figure 5. $k_{qpp}:k_d$ as a function of the pore size, temperature and pressure

As shown in Figure 5. The ratio is higher in small radius, especially pore radii below 5 nm. These results show one to two orders of magnitude change in permeability and explain the unusual gas production from these tight reservoir systems. As the pore size and reservoir pressure gradually increase, the shale pore characteristics are similar to those of traditional high permeability reservoirs, and the apparent permeability is gradually reduced to the Darcy permeability. The temperature has the lowest effect on permeability dynamic changes. Gas molecule movement and the collisions between molecules increase the apparent permeability under the high temperature. As a result, the apparent permeability should be carefully adjusted along with the production of shale reservoirs. Simultaneously, lab measurements must be performed under reservoir geological conditions as well as at different pressures and temperatures to generate a data bank of apparent permeability.

Reference:

[1] Wu, K. A model for multiple transport mechanisms through nanopores of shale gas reservoirs with real gas effect–adsorption-mechanic coupling. 2016.

[2] Chong, Z. Numerical investigation into the effect of natural fracture density on hydraulic fracture network propagation. Energies. 2017.

[3] Dian, Fan. Analytical model of gas transport in heterogeneous hydraulically-fractured organic-rich shale media. 2017.